



# Activated coconut shell charcoal based counter electrode for dye-sensitized solar cells

K.D.M.S.P.K. Kumarasinghe<sup>a,b</sup>, G.R.A. Kumara<sup>a,\*</sup>, R.M.G. Rajapakse<sup>b,c</sup>, D.N. Liyanage<sup>a,b</sup>,  
K. Tennakone<sup>d</sup>

<sup>a</sup> National Institute of Fundamental Studies, Hantana Road, Kandy 20000, Sri Lanka

<sup>b</sup> Postgraduate Institute of Science, University of Peradeniya, Peradeniya 20400, Sri Lanka

<sup>c</sup> Department of Chemistry, Faculty of Science, University of Peradeniya, Peradeniya 20400, Sri Lanka

<sup>d</sup> Department of Physics & Astronomy, Georgia State University, Atlanta, GA 30303, USA

## ARTICLE INFO

### Keywords:

Dye-sensitized solar cell  
Activated coconut shell charcoal  
Counter electrode

## ABSTRACT

Current studies on dye-sensitized solar cells are mainly focus on fabricating low-cost cell with high performances. Cost of dye-sensitized solar cells depends mainly on the counter electrode material where the best catalyst for triiodide reduction at the counter electrode is platinum, which is highly expensive. Among various non-platinum counter electrode catalysts, carbon-based materials stand out to be the best alternative as far as low-cost and ready abundance are concerned. A simple procedure is described for producing high electrical conductivity activated charcoal from coconut shells and depositing it on conducting tin oxide glass as a thin film, to be used as the counter electrode for dye-sensitized electrolytic solar cells. The activated coconut shell charcoal catalytic layer which is subjected to this work had very good adhesion between the particles as well as to the conducting tin oxide glass substrate. The efficiency of 7.85% obtained exceeds, values obtained from other forms of activated carbon derived from bio-materials.

## 1. Introduction

Dye-sensitized solar cells (DSCs) continue to attract attention gaining improvements in fabrication procedures and development of new dyes and redox electrolytes [1–4]. Recently an efficiency of 15% has been achieved [5]. Lowering the cost of fabrication and enhancing stability, will pave way for its commercialization. In addition to photo-induced electron injection to the TiO<sub>2</sub> matrix and transport across interconnected crystallites and hole scavenging by the iodide ions, the reversible functioning of electrolytic redox mediator depends on the counter electrode (CE) material and its structure. An essential quality of a CE is electrocatalytic activity towards triiodide reduction. The best known catalyst for triiodide reduction at the CE is platinum (Pt), which is expensive and also not entirely resistive to corrosion. The other important factor is the adherence of the catalytic material to the conducting glass surface, ensuring a good ohmic contact. Considering above requirements, different forms of carbon allotropes, inorganic materials and polymers have been examined [6–9]. Much effort is diverted in developing CEs based on readily available forms of carbon. Carbon based CEs are cheaper, non-toxic and resist iodine corrosion better than Pt. Carbon materials used are; graphite [10,11], carbon

black [12], carbon derived from pyrolysed sugars and activated charcoal derived from different biological materials [13–15], graphene [16] and carbon nanotubes [17,18]. Although, activated carbon based on biological materials are cheaper, they generally have lower electronic conductivities, compared to graphene and carbon nano-tubes.

In this note we describe a simple technique of fabrication of a CE based on highly conducting coconut shell charcoal, leading to an efficiency of 7.85%. According to knowledge of the authors this is the highest efficiency achieved in a DSC with a counter electrode based on carbon obtained by pyrolysis of a natural readily available bio-material. The detail of the method fabrication is described.

## 2. Material and methods

### 2.1. Preparation of activated coconut shell charcoal powder

Highly electrical conductivity porous activated charcoal was prepared from coconut shells abundant in Sri Lanka. Coconut shells were cleaned by scraping off the fibre and residue coconut pulp. The cleaned coconut shells were burnt in a metal chamber until flames originating from volatile matter ceases, displaying incandescence and quenched

\* Corresponding author.

E-mail address: [kumara.as@nifs.ac.lk](mailto:kumara.as@nifs.ac.lk) (G.R.A. Kumara).

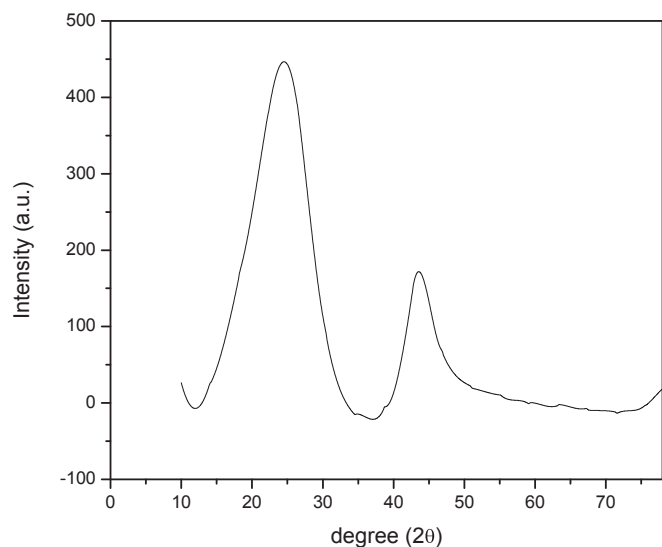


Fig. 1. X-ray Diffractogram of activated coconut shell charcoal prepared by the method described in the text.

Table 1

Data extracted from the XRD of ACSC shown in Fig. 1.

Peak Location 2θ (degrees)	Lattice Spacing d (Å)	FWHM	Crystallite Size, D (nm)	Material	Orientation
24.6547	3.6079	9.3270	87.12	C	002
43.7046	2.0694	4.8365	176.84	C	101

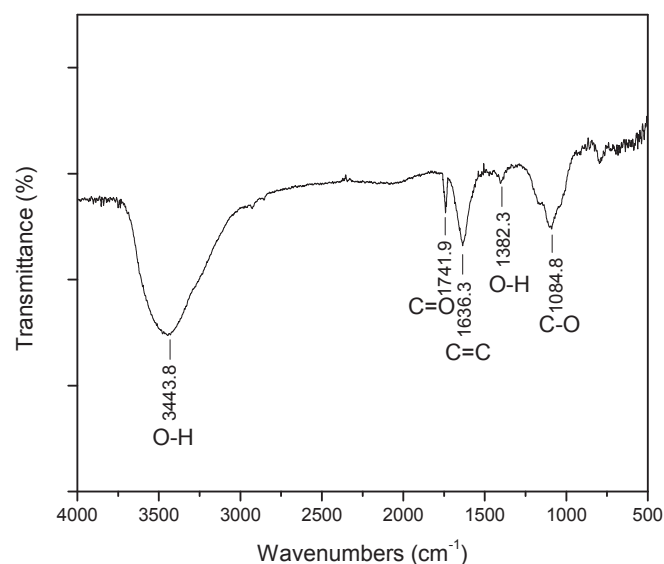


Fig. 2. FT-IR spectrum of as prepared ACSC powder.

Table 2

Characteristic IR band positions.

Maximum of the Absorption Band (cm <sup>-1</sup> )	Functional Group
3443.8	O-H stretching
1382.3	O-H bending
1741.9	C=O stretching
1636.3	C=C stretching
1084.8	C-O stretching

Table 3

Photovoltaic parameters of DSCs employing ACSC CE prepared with different amounts of PVA binder.

PVA amount added to 0.6 g of ACSC (mL)	J <sub>sc</sub> (mA cm <sup>-2</sup> )	V <sub>oc</sub> (V)	FF	η (%)
3	15.94	0.645	0.60	6.17
4	17.25	0.649	0.61	6.83
5	18.55	0.656	0.61	7.42
6	16.13	0.653	0.60	6.32
7	15.85	0.649	0.59	6.07

Table 4

Photovoltaic parameters of DSCs employing ACSC CEs sprayed at different temperatures of FTO.

Temperature of FTO substrate (°C)	J <sub>sc</sub> (mA cm <sup>-2</sup> )	V <sub>oc</sub> (V)	FF	η (%)
100	15.45	0.653	0.61	6.15
150	16.16	0.660	0.60	6.40
200	18.65	0.647	0.61	7.36
250	18.66	0.656	0.62	7.59
300	19.49	0.650	0.62	7.85
350	–	–	–	–

with water. The mineral material in the charcoal was eliminated by washing with 0.10 mol dm<sup>-3</sup> HCl several times, followed by distilled water and heated at 900 °C for 30 min in a box furnace. The hot charcoal was then dropped instantly into a distilled water tank, dried and ground into a powder. Activated coconut shell charcoal (ACSC) thus produced was characterized by XRD (Rigaku Ultima IV X-ray Diffractometer equipped with a Cu anode and dual detectors) and FT-IR.

## 2.2. Preparation of TiO<sub>2</sub> working electrode

Fluorine-doped tin oxide (FTO) plates (1 cm × 2 cm) were cleaned by ultra-sonication in a detergent for 5 min and thoroughly washed with distilled water and ethanol and allowed to dry under ambient conditions. Titanium tetraisopropoxide (8.0 mL) and acetic acid (1.0 mL) were mixed with ethanol (8.0 mL) and steam was passed through the solution in order to aid rapid hydrolysis. The expulsion of ethanol by steaming produced a transparent solid mass consisting of TiO<sub>2</sub> nanoparticles. The resultant solid mass was grounded with (20.0 mL) of de-ionized water in a motor and sonicated for 10 min. Finally, the dispersion was autoclaved at 150 °C for 3 h TiO<sub>2</sub> colloidal solution (30.0 mL), acetic acid (8.25 mL), Triton X-100 (8 drops) and ethanol (30.0 mL) was mixed thoroughly to prepare TiO<sub>2</sub> precursor. The precursor suspension was sprayed on to pre-heated (150 °C) FTO glass substrates using a purpose-built spray gun. TiO<sub>2</sub> film prepared in the above manner has thickness ~10 μm. Then TiO<sub>2</sub> sprayed plates were sintered at 500 °C for 30 min in air, allowed to cool down to 80 °C and kept soaked overnight in a 3 × 10<sup>-4</sup> mol dm<sup>-3</sup> solution of Ruthenium based N719 dye in a 1:1 v/v mixture of acetonitrile and *t*-butyl alcohol.

## 2.3. Preparation of activated coconut shell charcoal coated counter electrode

Polyvinyl acetate (PVA) binder was prepared by autoclaving PVA granular particles in de-ionized water at 150 °C for 3 h. Suspensions of ACSC were made by using 0.6 g of ACSC powder, 4 mL of ethanol and different amounts of PVA binder, sprayed onto FTO plates (using purpose-built spray gun) heated to different temperatures and sintered at 300 °C for 30 min in air. Then films were characterized by SEM. The electrical conductivity of ACSC layers were measured by four-probe method.

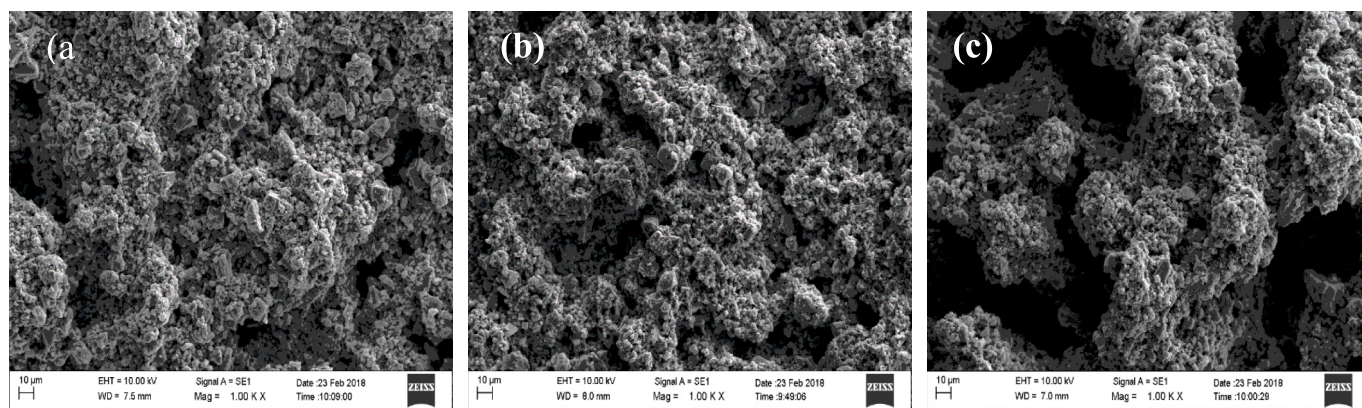


Fig. 3. SEM images of ASCS CE prepared at (a) 100 °C (b) 200 °C and (c) 300 °C.

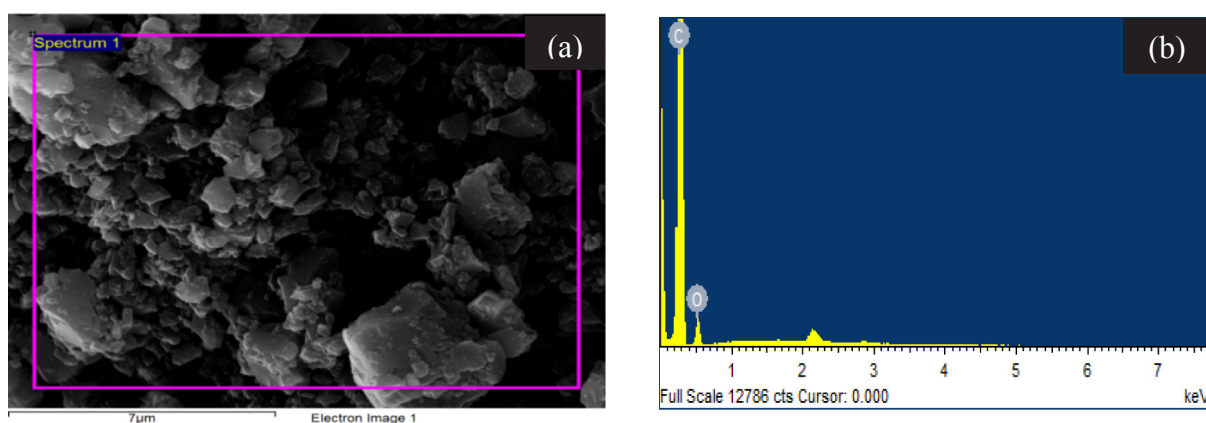


Fig. 4. (a) SEM image of activated coconut shell charcoal showing the area used in measuring elemental composition and (b) corresponding EDX spectrum.

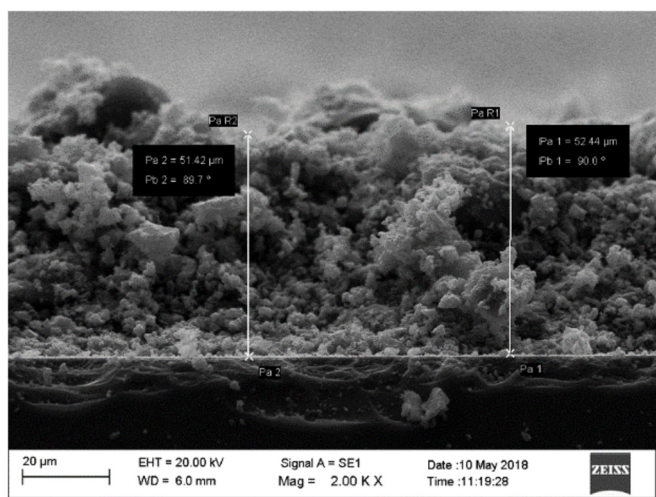


Fig. 5. Cross-sectional SEM image of the activated coconut shell charcoal layer on FTO glass.

#### 2.4. Construction of DSC

The electrolyte (0.10 mol dm<sup>-3</sup> LiI, 0.05 mol dm<sup>-3</sup> I<sub>2</sub>, 0.60 mol dm<sup>-3</sup> dimethylpropylimidazolium iodide and tertiarybutylpyridine in acetonitrile) impregnated as usual. A mask with a window of 0.25 cm<sup>2</sup> was also clipped on the working electrode. The efficiencies were measured at 100 mW cm<sup>-2</sup> AM 1.5 simulated sunlight

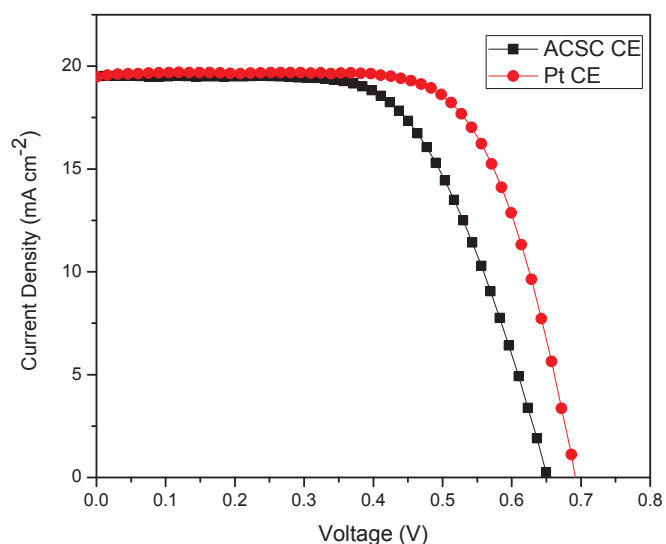


Fig. 6. J-V plots of the DSCs made from FTO-ACSC CE and usual FTO-Pt CE, under 1 sun illumination (AM 1.5, 100 mW cm<sup>-2</sup>).

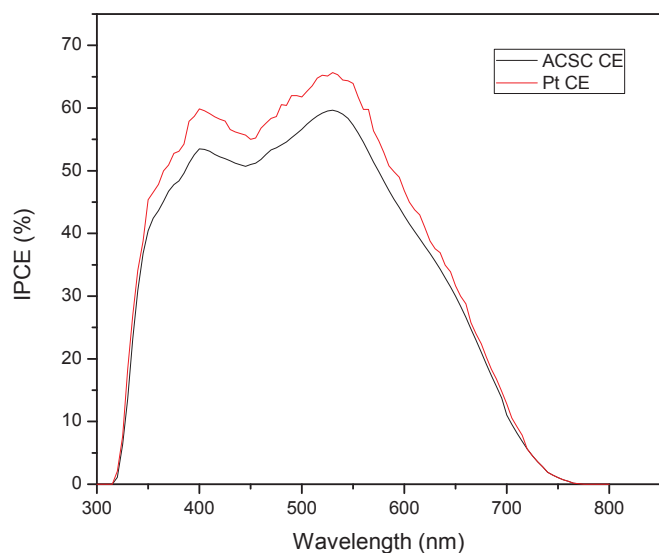


Fig. 7. IPCE Spectra of the DSCs fabricated using ACSC based CE and Pt-CE.

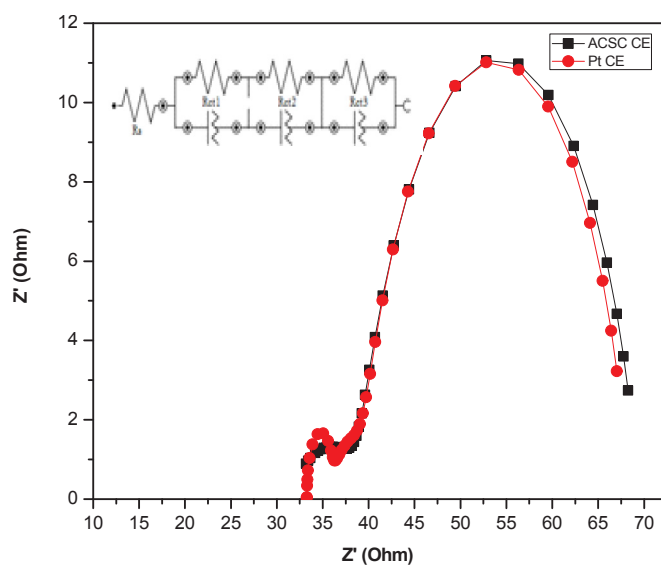


Fig. 8. Nyquist Plots of Electrochemical Impedance Spectra of DSCs fabricated using ACSC based CE and Pt-based CE.

using a home-made computer controlled set-up combined with Keithley 2000 multi-meter and a potentiostat/galvanostat HA-301.

### 3. Results and discussion

The X-Ray Diffractogram of the ACSC prepared in situ is given in Fig. 1. Relevant data extracted are given in Table 1.

Two broad bands centred at  $2\theta = 24.6547^\circ$  and  $2\theta = 43.7046^\circ$  indicate the poor crystallinity of the material and large crystallite sizes; 87.12 nm along (002) direction and 176.84 nm along (101) direction. This is very much similar to the XRD pattern of the activated carbon derived from orange peel [14] and that of commercially available activated carbon. The band centred at  $2\theta = 25^\circ$  can be assigned to be due to graphitic structure since (200) diffractions of graphite also appear in the same region.

Fig. 2 shows FT-IR spectrum of as prepared ACSC powder. Characteristic IR band positions are collected in Table 2.

After being carbonized, the as-prepared mesoporous active charcoal shows the stretching vibration absorption spectra of  $-\text{OH}$  at  $3443.8\text{ cm}^{-1}$ . The band centred at  $1741.9\text{ cm}^{-1}$  is due to the stretching

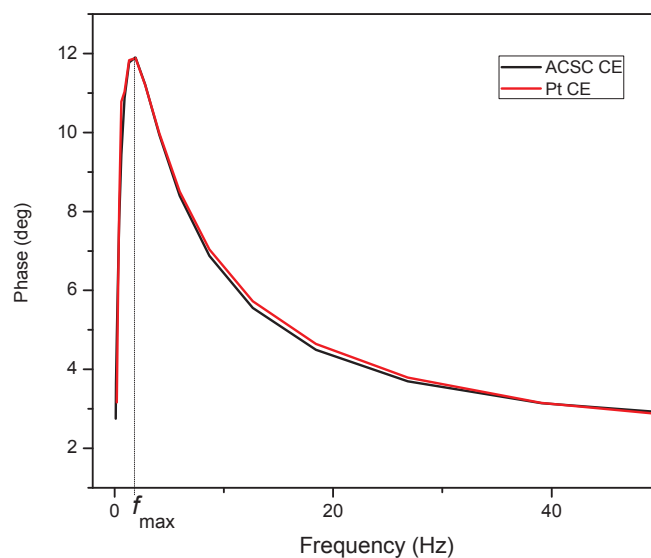


Fig. 9. Bode Plots for DSCs fabricated using ACSC based CE and Pt-based CE.

Table 5

Parameters used to fit EIS spectra of DSCs.

CE	$R_s$ ( $\Omega$ )	$R_{ct1}$ ( $\Omega$ )	$R_{ct2}$ ( $\Omega$ )	$f_{max}$	$\tau_c$ (ms)
ACSC	30.0	1.58	5.28	1.93	82.4
Pt	29.8	1.56	3.46	1.93	82.4

vibration absorption of  $\text{C}=\text{O}$ . This indicates that the mesoporous active charcoal contain hydroxyl, carbonyl products, methoxy and lactones. Absorption band of mesoporous active carbon in  $1636.3\text{ cm}^{-1}$  is due to stretching vibration of benzene ring skeleton. In addition, there is a small bending vibration peak of  $\text{O}-\text{H}$  at  $1382.3\text{ cm}^{-1}$  and  $\text{C}-\text{O}$  stretching vibration peak at  $1084.8\text{ cm}^{-1}$ .

The performance of ACSC CE was optimized by varying the amount of the PVA binder and the heating temperature of the FTO substrates. The photovoltaic parameters of fabricated DSCs are summarized in Table 3. The ACSC layers prepared using below 3 mL of PVA binder were peeled off.

Table 4 depicts the photovoltaic parameters obtained at different heating temperature of FTO. At the low substrate temperatures, large amount of the binder is exists in the CE material and it increases the resistance of ACSC CE which results the low efficiency. At the adequate temperatures, the PVA binder is burnt out to certain extend and provide a good adhesion between ACSC particles as well as ACSC particles to the FTO substrate which allows low resistance on ACSC CE. This results a high electrical conductivity and high performance of the cell. The highest efficiency gave at the substrate temperature of  $300^\circ\text{C}$ . As the substrate temperature increases over  $300^\circ\text{C}$ , binder burned out completely which tends to peeling off of ACSC films.

The SEM images of the ACSC thin film on FTO are shown in Fig. 3. Fig. 3(a), (b) and 3(c) show those prepared at  $100^\circ\text{C}$ ,  $200^\circ\text{C}$  and  $300^\circ\text{C}$  respectively.

As revealed from the SEM images, ACSC prepared at  $100^\circ\text{C}$ ,  $200^\circ\text{C}$  and  $300^\circ\text{C}$  have surface morphologies with spongy like appearance. Among them, the CE prepared at  $300^\circ\text{C}$  showing an excellent porous nature to possess high surface area. Particle sizes are in between 300 nm and  $1.7\text{ }\mu\text{m}$  though there are some aggregated aggregates of large particles are also present.

Fig. 4(a) shows the SEM image of as prepared ACSC (at  $300^\circ\text{C}$ ), together with its EDX spectrum [Fig. 4(b)]. EDX measures elements other than H and He and hence the amount H in the sample is not revealed in the data. EDX spectrum gives C 88.54% w/w (91.14% atomic %) and O 11.46% w/w (8.86% atomic %) so that at least one in

ten carbon atoms contain oxygen functionalities. These results agree well with those shown in FT-IR where functional groups such as –OH, COOH, epoxy etc. are present in this activated carbon.

The ACSC CE shows high electrical conductivity of  $4.72 \times 10^3 \text{ S m}^{-1}$  at room temperature measured by four-probe method. Using this activated charcoal, CEs for DSCs were fabricated by attaching these particles on a transparent, conducting, FTO layer on glass, from the procedure outlined in the experimental section. The cross-sectional SEM of the CEs is shown in Fig. 5. The thickness of the ACSC layer on FTO can be estimated to be 52  $\mu\text{m}$ .

In Fig. 6, the *J-V* curve of the DSC with the ACSC CE is compared with that of the otherwise identical DSC except that the CE used is usual FTO-Pt.

The DSC with FTO-Pt CE gives  $J_{\text{sc}}$  of 19.52  $\text{mA cm}^{-2}$ ,  $V_{\text{OC}}$  of 0.689 V and FF of 0.70 giving rise to the conversion efficiency of 9.41% whereas the DSC with ACSC gives the corresponding values of 19.49  $\text{mA cm}^{-2}$ ,  $V_{\text{OC}}$  of 0.650 V and FF of 0.62 giving rise to the conversion efficiency of 7.85%. Although, both DSCs give similar short circuit current densities, 17% lower efficiency obtained for the DSC with ACSC based CE from that of Pt-based CE is due to slightly lower  $V_{\text{OC}}$  and FF.

Depicted in Fig. 7 are the IPCE spectra of DSCs fabricated using counter electrodes made ACSC that gives the best efficiency and standard Pt. At each wavelength it is apparent that the Pt-CE based DSC gives slightly higher IPCE than that based on ACSC.

In order to understand the performances of two types of DSCs their Electrochemical Impedance Spectra (EIS) were studied. Fig. 8 depicts the Nyquist plots of DSCs fabricated using ACSC CE and Pt-CE measured between  $1 \times 10^{-2}$  –  $1 \times 10^6$  Hz under 1 sun illumination (AM 1.5, 100  $\text{mW cm}^{-2}$ ) and equivalent circuit diagram which fitted with NOVA software is shown in the inset of the Figure. Fig. 9 depicts Bode Plots for DSCs fabricated using ACSC based CE and Pt-based CE. The ohmic series resistance ( $R_s$ ) corresponds to the overall series resistance. Both Nyquist plot contains two semi circles: the larger semi-circle belongs to the charge transport/accumulation resistance at dye anchored  $\text{TiO}_2$ /electrolyte interface ( $R_{\text{ct}2}$ ) and the smaller semi-circle is related to the charge transfer resistance at CE/electrolyte interface ( $R_{\text{ct}1}$ ).

Table 5 depicts the calculated values of Ohmic series resistance ( $R_s$ ), Charge transfer resistance at CE/electrolyte interface ( $R_{\text{ct}1}$ ), Charge transport/accumulation resistance at dye anchored  $\text{TiO}_2$ /electrolyte interface ( $R_{\text{ct}2}$ ),  $f_{\text{max}}$ , and electron life time ( $\tau_e$ ) based on equivalent circuits and extracted from the Bode plots.

Both the charge transfer resistance at CE/electrolyte interface ( $R_{\text{ct}1}$ ) and charge transport/accumulation resistance at dye anchored  $\text{TiO}_2$ /electrolyte interface ( $R_{\text{ct}2}$ ) are slightly higher when ACSC is used as CE in place of Pt. This is also manifested by slightly higher series resistance of the former cell when compared to that of the latter cell. These factors may account for the slightly lower performance of the DSC with ACSC CE when compared to that of DSC based on Pt-CE.

#### 4. Conclusion

A method has been developed to produce highly conducting activated coconut charcoal and deposit on conducting tin oxide glass to fabricate a counter electrode for a dye-sensitized solar cell. The efficiency obtained is highest reported for CE based on a natural carbon material. Coconuts shells are readily available and extensively used for manufacture of activated charcoal used in diverse variety of applications. The activation procedures commonly adopted are energy intensive involving several processing steps. Procedure adopted here is relatively simple. Heating the burnt shell in air for 20–30 min at 900 °C, effectively pyrolyse all organic components to carbon, except for introduction surface groups. It is not clear whether surface ligands play any role in electrocatalytic activity or adherence of the material to the conducting glass. The absorption band in FTIR at 1741.9  $\text{cm}^{-1}$  seems to

originate from C=C stretching of carboxylate. This ligand binds to oxide semiconductors (i.e.  $\text{SnO}_2$  in FTO). However, direct evidence for binding of activated charcoal to FTO surface via carboxylate could not be ascertained. CE made from coconut shell charcoal by the method described in this work was found to be superior to best coconut shell and other forms of activated carbon. The reason appears to be high electrical conductivity and good electrocatalytic activity towards triiodide reduction.

#### Acknowledgements

The authors would like to thank the National Institute of Fundamental Studies, Sri Lanka for financial support.

#### References

- [1] K. Hara, H. Arakawa, Handbook of Photovoltaic Science and Engineering, John Wiley & Sons, Ltd, Chichester, UK, 2003, <https://doi.org/10.1002/0470014008>.
- [2] S. Ito, T.N. Murakami, P. Comte, P. Liska, C. Grätzel, M.K. Nazeeruddin, M. Grätzel, Fabrication of thin film dye sensitized solar cells with solar to electric power conversion efficiency over 10%, Thin Solid Films 516 (2008) 4613–4619, <https://doi.org/10.1016/j.tsf.2007.05.090>.
- [3] J.M. Cole, T.E. Simos, G. Psihoyios, C. Tsitouras, Z. Anastassi, Systematic prediction of dyes for dye sensitized solar cells: data-mining via molecular charge-transfer algorithms, AIP Conf. Proc, 2011, pp. 999–1002, <https://doi.org/10.1063/1.3637778>.
- [4] M. Wang, C. Grätzel, S.M. Zakeeruddin, M. Grätzel, Recent developments in redox electrolytes for dye-sensitized solar cells, Energy Environ. Sci. (2012), <https://doi.org/10.1039/C6EE00811A>.
- [5] K. Kakiage, Y. Aoyama, T. Yano, K. Oya, J. Fujisawa, M. Hanaya, Highly-efficient dye-sensitized solar cells with collaborative sensitization by silyl-anchor and carboxy-anchor dyes, Chem. Commun. 51 (2015) 15894–15897, <https://doi.org/10.1039/C5CC06759F>.
- [6] S.S. Khalili, H. Dehghani, M. Afroz, Composite films of metal doped CoS/carbon allotropes; efficient electrocatalyst counter electrodes for high performance quantum dot-sensitized solar cells, J. Colloid Interface Sci. 493 (2017) 32–41, <https://doi.org/10.1016/j.jcis.2017.01.005>.
- [7] M. Wu, T. Ma, Platinum-free catalysts as counter electrodes in dye-sensitized solar cells, ChemSusChem 5 (2012) 1343–1357, <https://doi.org/10.1002/cssc.201100676>.
- [8] A. Ramachandran, I. Jinchu, C.O. Sreekala, Studies on polymer based counter electrodes for DSSC application, 2016 Int. Conf. Electr. Electron. Optim. Tech, IEEE, 2016, pp. 4628–4630, <https://doi.org/10.1109/ICEEOT.2016.7755595>.
- [9] P. Veerender, V. Saxena, A. Gusain, P. Jha, S.P. Koiry, A.K. Chauhan, D.K. Aswal, S.K. Gupta, Conducting Polymers Based Counter Electrodes for Dye-Sensitized Solar Cells, (2014), pp. 1048–1050, <https://doi.org/10.1063/1.4872848>.
- [10] E.N. Jayaweera, G.R.A. Kumara, H.M.G.T.A. Pitawala, R.M.G. Rajapakse, N. Gunawardhana, H.M.N. Bandara, A. Senarathne, C.S.K. Ranasinghe, H.-H. Huang, M. Yoshimura, Vein graphite-based counter electrodes for dye-sensitized solar cells, J. Photochem. Photobiol. A Chem. 344 (2017) 78–83, <https://doi.org/10.1016/j.jphotochem.2017.05.009>.
- [11] Y.-Y. Li, C.-T. Li, M.-H. Yeh, K.-C. Huang, P.-W. Chen, R. Vittal, K.-C. Ho, Graphite with different structures as catalysts for counter electrodes in dye-sensitized solar cells, Electrochim. Acta 179 (2015) 211–219, <https://doi.org/10.1016/j.electacta.2015.06.007>.
- [12] T.N. Murakami, S. Ito, Q. Wang, M.K. Nazeeruddin, T. Bessho, I. Cesar, P. Liska, R. Humphry-Baker, P. Comte, P. Péchy, M. Grätzel, Highly efficient dye-sensitized solar cells based on carbon black counter electrodes, J. Electrochem. Soc. 153 (2006) A2255, <https://doi.org/10.1149/1.2358087>.
- [13] R. Kumar, S.S. Nemala, S. Mallick, P. Bhargava, Synthesis and characterization of carbon based counter electrode for dye sensitized solar cells (DSSCs) using sugar free as a carbon material, Sol. Energy 144 (2017) 215–220, <https://doi.org/10.1016/j.solener.2017.01.030>.
- [14] Z. Xie, W. Guan, F. Ji, Z. Song, Y. Zhao, Production of biologically activated carbon from orange peel and landfill leachate subsequent treatment technology, J. Chem. 2014 (2014) 1–9, <https://doi.org/10.1155/2014/491912>.
- [15] R. Madhu, V. Veeramani, S.-M. Chen, J. Palanisamy, A.T. Ezhil Vilian, Pumpkin stem-derived activated carbons as counter electrodes for dye-sensitized solar cells, RSC Adv. 4 (2014) 63917–63921, <https://doi.org/10.1039/C4RA12585A>.
- [16] H. Wang, Y.H. Hu, Graphene as a counter electrode material for dye-sensitized solar cells, Energy Environ. Sci. 5 (2012) 8182, <https://doi.org/10.1039/c2ee21905k>.
- [17] S. Huang, H. Sun, X. Huang, Q. Zhang, D. Li, Y. Luo, Q. Meng, Carbon nanotube counter electrode for high-efficient fibrous dye-sensitized solar cells, Nanoscale Res. Lett. 7 (2012) 222, <https://doi.org/10.1186/1556-276X-7-222>.
- [18] J.G. Nam, Y.J. Park, B.S. Kim, J.S. Lee, Enhancement of the efficiency of dye-sensitized solar cell by utilizing carbon nanotube counter electrode, Scripta Mater. 62 (2010) 148–150, <https://doi.org/10.1016/j.scriptamat.2009.10.008>.